

First-Principles Study of Double Perovskite Sr_2FeXO_6 ($X=\text{Mo}, \text{Re}$) Ultrathin Films and Heterostructures

Shugo Suzuki and Makoto Tsuyama

*Division of Materials Science, Faculty of Pure and Applied Sciences, University of Tsukuba,
Tsukuba, Ibaraki 305-8573, Japan*

We study double perovskite Sr_2FeXO_6 ($X=\text{Mo}, \text{Re}$) ultrathin films (UTFs) and their heterostructures with a SrTiO_3 substrate by first-principles calculations based on density functional theory. It is found that the UTFs and their heterostructures are all half-metallic despite being extremely thin.

1. Introduction

In the last two decades, spintronics has developed into a field of intensive research.¹⁾ Spintronics exploits not only the electron charge but also its spin.²⁾ In spintronic devices such as magnetoresistive random access memory, magnetic tunnel junctions are one of the most important building blocks, consisting of an insulating layer sandwiched by two ferromagnetic ultrathin films (UTFs) in their most basic form. Of great importance for magnetic tunnel junctions is the tunnel magnetoresistance (TMR) effect.^{3–6)}

In widely studied magnetic tunnel junctions, the insulating layer and ferromagnetic UTFs are made of crystalline MgO and 3d transition metals such as Fe, Co, and CoFe alloys, respectively. This combination of the insulating layer and ferromagnetic UTFs has succeeded in achieving a TMR ratio of over 500% at room temperature;^{7–11)} the giant TMR effect originates from the coherent tunneling of fully spin-polarized electrons in the ferromagnetic UTFs through the MgO insulating layer.^{12–14)}

An alternative class of ferromagnetic materials for which a large TMR effect is expected is half metals, which have attracted a lot of attention due to their possible applications in spintronics.^{15–22)} A half metal is a material that behaves as a conductor to electrons of one spin orientation but as an insulator to those of the opposite spin orientation. Well-known half metals are Heusler alloys,¹⁵⁾ chromium dioxide,^{16,17)} magnetite,^{18,19)} transition-metal chalcogenides and pnictides,²⁰⁾ manganese perovskite oxides,²¹⁾ and double perovskites.²²⁾

Among them, double perovskites have attracted much attention in oxide spintronics, with

rich functionalities expected in the UTFs and their heterostructures. Double perovskites are compounds with a general chemical formula of $A_2BB'O_6$, where A is usually an alkaline-earth metal atom or rare-earth metal atom while B is a $3d$ transition metal atom and B' is a $4d$ or $5d$ transition-metal atom. The TMR effect in $\text{Sr}_2\text{FeMoO}_6$ (SFMO) at room temperature was found by Kobayashi et al.²²⁾ They showed that SFMO is a half-metallic ferromagnet with a Curie temperature of 415 K, high enough for the application to spintronic devices at room temperature. In SFMO, the spin magnetic moments (M_{spin}) of Fe^{3+} and Mo^{5+} atoms are antiferromagnetically coupled to each other. The structural, electronic, and magnetic properties of the bulk double perovskites have been studied extensively.^{23–39)}

At the same time, experimental studies of the double-perovskite films have been performed;^{40–55)} in most of these studies, a SrTiO_3 (STO) substrate was used for thin-film growth. On the other hand, there have been very few theoretical studies of double-perovskite UTFs. To the best of our knowledge, the only theoretical study is the pioneering work on SFMO UTFs by Zhang et al.⁵⁵⁾ A theoretical study of double-perovskite UTFs also seems important because the ferromagnetic UTFs are a crucial ingredient of any spintronic device. Note that at the surfaces and interfaces of Heusler alloys, the half-metallicity is in general lost due to the surface or interface states;^{56,57)} this is the reason why surface- and interface-sensitive probes do not find 100% spin polarization in Heusler alloy films.^{17,58)} Thus, it is indispensable to study whether double-perovskite UTFs remain half-metallic or not.

The purpose of this work is to investigate the structural, electronic, and magnetic properties of the UTFs of the double perovskite Sr_2FeXO_6 (SFXO), where $X=\text{Mo, Re}$, and their heterostructures with the STO substrate by first-principles calculations based on density functional theory. The method of calculations is explained in Sect. 2. The results and discussion are given in Sect. 3. Finally, we give the conclusions of this work in Sect. 4.

2. Method of Calculations

The models for the SFXO UTFs and their heterostructures studied in this work are schematically shown in Fig. 1. For all the models, we assume a two-dimensional square lattice with the in-plane lattice constant $a=5.57 \text{ \AA}$, which corresponds to the lattice constant of bulk SFXO, and $a=5.52 \text{ \AA}$, which corresponds to the lattice constant of the STO substrate; note that the lattice mismatch between SFXO and STO is very small, i.e., about 1%. Model I is a slab of three atomic layers, in which the FeXO_4 layer is sandwiched by two SrO layers. Model II is a slab of five atomic layers, consisting of two FeXO_4 layers and three SrO layers. Model III is also a slab of five atomic layers but is different from model II in that model III

represents the heterostructure of the SFXO UTFs with the STO substrate.

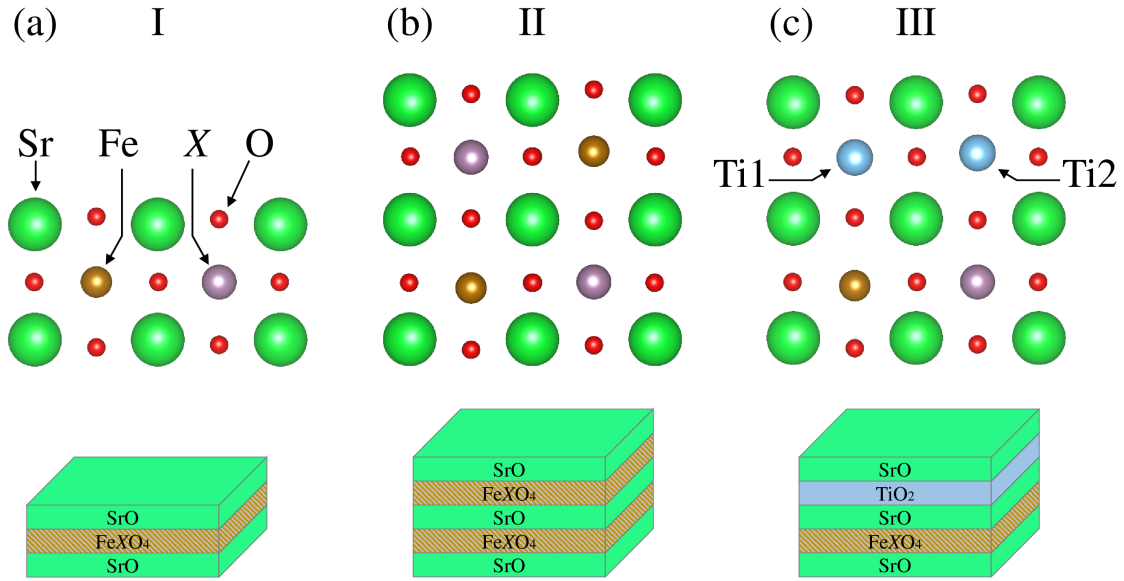


Fig. 1. (Color online) Schematic diagram of models (a) I, (b) II, and (c) III. For all the models, we assume a two-dimensional square lattice with the in-plane lattice constant $a=5.57 \text{ \AA}$, which corresponds to the lattice constant of bulk SFXO, and $a=5.52 \text{ \AA}$, which corresponds to the lattice constant of the STO substrate. Model I is a slab of three atomic layers, in which the FeXO_4 layer is sandwiched by two SrO layers. Model II is a slab of five atomic layers, consisting of two FeXO_4 layers and three SrO layers. Model III is also a slab of five atomic layers but is different from model II in that model III represents the heterostructure of the SFXO ultrathin films with the STO substrate.

We carried out all-electron calculations using the scalar relativistic full-potential linear-combination-of-atomic-orbitals (SFLCAO) method and the fully relativistic full-potential linear-combination-of-atomic-orbitals (FFLCAO) method, both based on density functional theory.^{59–61)} To calculate the electrostatic potential we used the two-dimensional Ewald method.^{62,63)} We first optimized the structures of the systems using the SFLCAO method with the generalized gradient approximation (GGA) to the exchange-correlation energy functional; we used the Perdew–Burke–Ernzerhof form of the GGA to optimize the structures.⁶⁴⁾ Using the optimized structures, the electronic and magnetic properties of the systems were calculated as follows. The densities of states (DOS) and M_{spin} were calculated using the SFLCAO method with the GGA+ U approach,^{65,66)} the on-site Coulomb repulsion U_{eff} was taken into account using the simplified approach proposed by Dudarev et al.⁶⁶⁾ We used the effective U_{eff} parameters of 4 eV for the Fe 3d orbitals and 2 eV for the Ti 3d orbitals;^{28,67)} we did not consider the on-site Coulomb repulsion for the Mo 4d or Re 5d orbitals. The magnetic

anisotropy energy (MAE) was calculated using the FFLCAO method within the local spin density approximation; we used the Perdew–Wang parameterization of the Ceperley–Alder results.^{68,69)} The MAE calculated in this work is the difference between the total energy for the in-plane magnetization, $E_{\text{tot}}^{[100]}$, and that for the perpendicular magnetization, $E_{\text{tot}}^{[001]}$. We adopt the definition that the positive (negative) MAE corresponds to the perpendicular (in-plane) magnetic anisotropy, i.e., $\text{MAE} = E_{\text{tot}}^{[100]} - E_{\text{tot}}^{[001]}$. We do not consider the contribution of the shape magnetic anisotropy originating from the magnetic dipole-dipole interaction.

The atomic orbitals used as the basis functions are as follows: the $1s$, $2s$, $2p$, $3s$, $3p$, $3d$, $4s$, $4p$, and $5s$ orbitals of the neutral Sr atom; the $5s$ and $5p$ orbitals of the Sr^{2+} atom; the $4d$ orbitals of the Sr^{4+} atom; the $1s$, $2s$, $2p$, $3s$, $3p$, $3d$, and $4s$ orbitals of the neutral Ti and Fe atoms; the $3d$, $4s$, and $4p$ orbitals of the Ti^{2+} and Fe^{2+} atoms; the $1s$, $2s$, $2p$, $3s$, $3p$, $3d$, $4s$, $4p$, $4d$, and $5s$ orbitals of the neutral Mo atom; the $5s$ and $5p$ orbitals of the Mo^{2+} atom; the $4d$ orbitals of the Mo^{4+} atom; the $1s$, $2s$, $2p$, $3s$, $3p$, $3d$, $4s$, $4p$, $4d$, $4f$, $5s$, $5p$, $5d$, and $6s$ orbitals of the neutral Re atom; the $6s$ and $6p$ orbitals of the Re^{2+} atom; and the $5d$ orbitals of the Re^{6+} atom. Note that the use of the atomic orbitals of positively charged atoms as well as those of neutral atoms is crucial to describing the contraction of atomic orbitals associated with cohesion. The Brillouin zone integration in the self-consistent field calculations was carried out using the good-lattice-point method;⁷⁰⁾ we used 34 k points to optimize the structures and 89 k points to calculate the MAE. The densities of states were calculated using the 11×11 k -point mesh in the full Brillouin zone. To speed up the convergence, we used a Fermi distribution smearing of eigenstates with a width of 30 meV. We used the force criterion of $0.01 \text{ eV}/\text{\AA}$ to stop the structure optimization.

3. Results and Discussion

We begin with the optimized structures of models I, II, and III. The results are shown in Table I. For comparison, the optimized structures of the bulk SFXO are also shown in the table together with those reported in previous experimental and theoretical studies; we assumed the structure of the bulk SFRO to be $Fm\bar{3}m$ to compare with the previous theoretical results reported by Zhang and Ji,³⁷⁾ although its actual structure is more complicated.³⁵⁾ In the table, the lengths of the M -O bonds, where $M = \text{Fe}$, Mo , Re , Ti1 , and Ti2 , are given. The notations for the lengths are shown in Fig. 2. The M -O bonds in the film plane are denoted by $M\text{-O}_{\parallel}$. The M -O bonds perpendicular to the film plane are denoted by $M\text{-O}_{\perp}^{\text{out}}$ or $M\text{-O}_{\perp}^{\text{in}}$, where the superscript “out” means that the O atom is in the outermost SrO layer while the superscript “in” means that the O atom is in the middle SrO layer. Note that there are no

$M-O_{\perp}^{\text{in}}$ bonds in model I. In Table I, the in-plane and perpendicular diagonals of the MO_6 octahedra are also shown; the in-plane diagonal, $d_{\parallel}^{MO_6}$, is twice the length of the $M-O_{\parallel}$ bond while the perpendicular diagonal, $d_{\perp}^{MO_6}$, is the sum of the lengths of the $M-O_{\perp}^{\text{out}}$ and $M-O_{\perp}^{\text{in}}$ bonds, except for in model I, where $d_{\perp}^{MO_6}$ represents twice the length of the $M-O_{\perp}^{\text{out}}$ bond. For $M=\text{Ti1}$ and Ti2 in model III, we show the lengths of the Ti1-O and Ti2-O bonds and the diagonals of the Ti1O_6 and Ti2O_6 octahedra in parentheses.

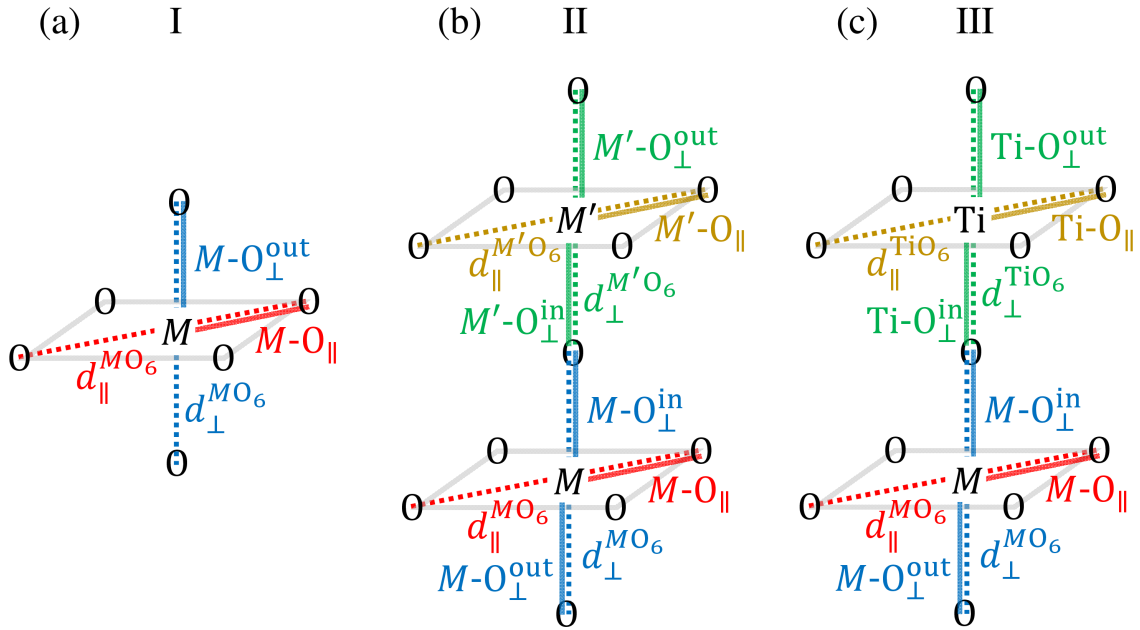


Fig. 2. (Color online) Schematic diagram of the MO_6 octahedra in models (a) I, (b) II, and (c) III. M (M') represents Fe, Mo, and Re; note that the Ti atom is shown explicitly. The M -O bonds are drawn with thick solid lines while the diagonals of the MO_6 octahedra are drawn with thick dotted lines. The M -O bonds in the film plane are denoted by $M-O_{\parallel}$. The M -O bonds perpendicular to the film plane are denoted by $M-O_{\perp}^{\text{out}}$ or $M-O_{\perp}^{\text{in}}$, where the superscript “out” means that the O atom is in the outermost SrO layer while the superscript “in” means that the O atom is in the middle SrO layer; note that there are no $M-O_{\perp}^{\text{in}}$ bonds in model I. The in-plane diagonal, $d_{\parallel}^{MO_6}$, is twice the length of the $M-O_{\parallel}$ bond while the perpendicular diagonal, $d_{\perp}^{MO_6}$, is the sum of the lengths of the $M-O_{\perp}^{\text{out}}$ and $M-O_{\perp}^{\text{in}}$ bonds, except for in model I, where $d_{\perp}^{MO_6}$ represents twice the length of the $M-O_{\perp}^{\text{out}}$ bond.

To verify the reliability of our optimized structures, we first compare the optimized structures of the bulk SFXO with the results of the previous experimental and theoretical studies shown in Table I.^{22, 24, 37)} For the bulk SFMO, our calculated $d_{\parallel}^{\text{FeO}_6}$ and $d_{\perp}^{\text{FeO}_6}$ are found to be equal, 3.99 Å, and our calculated $d_{\parallel}^{\text{MoO}_6}$ and $d_{\perp}^{\text{MoO}_6}$ are also found to be equal, 3.89 Å. The results of this work are in agreement with those of the previous experimental studies; the

experimental $d_{\parallel}^{\text{FeO}_6}$ and $d_{\perp}^{\text{FeO}_6}$ reported in Ref. 22 are 4.00 and 4.02 Å, and those reported in Ref. 24 are 3.96 and 4.00 Å, respectively. For the bulk SFRO, where $d_{\parallel}^{\text{FeO}_6}$ is equal to $d_{\perp}^{\text{FeO}_6}$ according to the $Fm\bar{3}m$ symmetry, we find $d_{\parallel}^{\text{FeO}_6}$ ($=d_{\perp}^{\text{FeO}_6}$) to be 4.01 Å and $d_{\parallel}^{\text{ReO}_6}$ ($=d_{\perp}^{\text{ReO}_6}$) to be 3.88 Å. The results of this work are in good agreement with those reported in the previous theoretical study by Zhang and Ji,³⁷⁾ $d_{\parallel}^{\text{FeO}_6}$ ($=d_{\perp}^{\text{FeO}_6}$) is 4.02 Å while $d_{\parallel}^{\text{ReO}_6}$ ($=d_{\perp}^{\text{ReO}_6}$) is 3.88 Å. Thus, the error of our optimized structure is expected to be about 1%. Note that the MO_6 octahedra are regular in the bulk SFXO.

We now examine the optimized structures of models I, II, and III. It is found that the FeO_6 octahedra in all the models are elongated considerably along the perpendicular direction. The perpendicular diagonal $d_{\perp}^{\text{FeO}_6}$, which is about 4.2 Å, is about 0.2 Å longer than the in-plane diagonal $d_{\parallel}^{\text{FeO}_6}$, which is about 4.0 Å. The XO_6 octahedra are also elongated along the perpendicular direction; $d_{\perp}^{\text{XO}_6}$ is about 4.0 Å and $d_{\parallel}^{\text{XO}_6}$ is about 3.9 Å. Such distortion of the FeO_6 and XO_6 octahedra is not found in the bulk SFXO, in which the FeO_6 and XO_6 octahedra are regular as mentioned above. Thus, it is most likely that the distortion of the FeO_6 and XO_6 octahedra is one of the characteristics of the SFXO UTFs.

To gain insight into the mechanism of the distortion of the FeO_6 octahedra in the SFXO UTFs, we carried out the structure optimization of a slab model consisting of three atomic layers similar to model I; in this slab model the Fe and Mo atoms in model I are replaced by two Ti atoms. The results of the structure optimization showed that $d_{\parallel}^{\text{TiO}_6}$ and $d_{\perp}^{\text{TiO}_6}$ are 3.94 and 3.98 Å, respectively; the distortion of the TiO_6 octahedra is smaller than that of the FeO_6 octahedra in the SFXO UTFs. Note that the reason why $d_{\perp}^{\text{TiO}_6}$ is longer than $d_{\parallel}^{\text{TiO}_6}$ by 0.04 Å may be that the O atoms in the outermost SrO layers can easily move toward the vacuum region outside. This is likely the case for the FeO_6 octahedra in the SFXO UTFs. Moreover, in octahedral coordination the ionic radius of the Fe^{3+} atom is larger than that of the Ti^{4+} atom by about 0.05 Å. Thus, these reasons may explain almost all of the difference between $d_{\perp}^{\text{FeO}_6}$ and $d_{\parallel}^{\text{FeO}_6}$ in the SFXO UTFs.

In models II and III, another kind of distortion of the MO_6 octahedra from regular octahedra is found to occur. The $\text{Fe-O}_{\perp}^{\text{out}}$ bonds are shorter than the $\text{Fe-O}_{\perp}^{\text{in}}$ bonds while the $X\text{-O}_{\perp}^{\text{out}}$ bonds are longer than the $X\text{-O}_{\perp}^{\text{in}}$ bonds. That is, the Fe atoms in the FeO_6 octahedra in models II and III are at off-center positions of the octahedra and are about 0.2 Å outward from the center, while the X atoms in the XO_6 octahedra are at off-center positions and are about 0.1 Å inward from the center. As a result, the FeXO_4 layer shows rumpling in which the Fe atoms are displaced further outward than the X atoms by about 0.3 Å. This is another characteristic of the SFXO UTFs not found in the bulk SFXO.

Also there are some characteristics of the SFXO UTFs common to the bulk SFXO. It is found that the Fe-O_{\parallel} bond is longer than the X-O_{\parallel} bond by about 0.05 \AA for all the models; this is a characteristic common to the bulk SFXO. In the SFXO UTFs, the Fe-O_{\parallel} bond lengths are about 2.00 \AA while the X-O_{\parallel} bond lengths are about 1.95 \AA . For both $\text{X}=\text{Mo}$ and Re , this is consistent with the fact that in the bulk SFXO, the Fe-O bond length, 2.00 \AA , is longer than the X-O bond length, 1.95 \AA .

It is interesting to note that the difference between the $\text{Fe-O}_{\perp}^{\text{out}}$ and $\text{Fe-O}_{\perp}^{\text{in}}$ bond lengths in model II with $\text{X}=\text{Mo}$ and $a=5.57$ (5.52) \AA is 0.25 (0.24) \AA , while that in model III is 0.17 (0.01) \AA and that the difference between the $\text{Mo-O}_{\perp}^{\text{out}}$ and $\text{Mo-O}_{\perp}^{\text{in}}$ bond lengths in model II is 0.07 (0.08) \AA while that in model III is 0.02 (0.01) \AA . This means that the STO layer relaxes the degree of distortion of the FeO_6 and MoO_6 octahedra at the interface. In particular, in model III with $a=5.52 \text{ \AA}$, the Fe atom is almost at the center of the FeO_6 octahedron. The same trend can be found for the systems with $\text{X}=\text{Re}$; the difference between the $\text{Fe-O}_{\perp}^{\text{out}}$ and $\text{Fe-O}_{\perp}^{\text{in}}$ bond lengths in model II with $\text{X}=\text{Re}$ and $a=5.57$ (5.52) \AA is 0.24 (0.27) \AA while that in model III is 0.13 (0.14) \AA , and the difference between the $\text{Re-O}_{\perp}^{\text{out}}$ and $\text{Re-O}_{\perp}^{\text{in}}$ bond lengths in model II is 0.05 (0.06) \AA while that in model III is 0.02 (0.02) \AA . On the other hand, the distortion of the Ti1O_6 and Ti2O_6 octahedra is small; the small distortion may be induced by the distortion of the FeO_6 and XO_6 octahedra.

Table I. Bond lengths of the in-plane and perpendicular M -O ($M=\text{Fe, Mo, Re, Ti1, and Ti2}$) bonds as well as the in-plane and perpendicular diagonals of the MO_6 octahedra (in Å) for models I, II, and III, together with those for the bulk SFMO. The in-plane M -O bonds are denoted by $M-O_{\parallel}$. The perpendicular M -O bonds are denoted by $M-O_{\perp}^{\text{out}}$ and $M-O_{\perp}^{\text{in}}$, where the superscript “out” means that the O atom is in the outermost SrO layer while the superscript “in” means that the O atom is in the middle SrO layer. The in-plane and perpendicular diagonals of the MO_6 octahedra are denoted by $d_{\parallel}^{MO_6}$ and $d_{\perp}^{MO_6}$, respectively. For $M=\text{Ti1 and Ti2}$ in model III, the lengths of the Ti1-O and Ti2-O bonds and the diagonals of the Ti1O₆ and Ti2O₆ octahedra are shown in parentheses.

X	System	a	Fe- O_{\parallel} (Ti1- O_{\parallel})	Fe- O_{\perp}^{out} (Ti1- O_{\perp}^{out})	Fe- O_{\perp}^{in} (Ti1- O_{\perp}^{in})	$d_{\parallel}^{\text{FeO}_6}$ ($d_{\parallel}^{\text{Ti1O}_6}$)	$d_{\perp}^{\text{FeO}_6}$ ($d_{\perp}^{\text{Ti1O}_6}$)	$X-O_{\parallel}$ (Ti2- O_{\parallel})	$X-O_{\perp}^{\text{out}}$ (Ti2- O_{\perp}^{out})	$X-O_{\perp}^{\text{in}}$ (Ti2- O_{\perp}^{in})	$d_{\parallel}^{XO_6}$ ($d_{\parallel}^{\text{Ti2O}_6}$)	$d_{\perp}^{XO_6}$ ($d_{\perp}^{\text{Ti2O}_6}$)
Mo	model I	5.57	1.99	2.10	3.98	4.20	1.95	2.01	3.90	4.02		
		5.52	1.97	2.12	3.94	4.24	1.93	2.02	3.86	4.04		
	model II	5.57	1.99	1.98	2.23	3.98	4.21	1.95	2.03	1.96	3.90	3.99
		5.52	1.97	2.00	2.24	3.94	4.24	1.94	2.04	1.96	3.88	4.00
	model III	5.57	2.00	2.01	2.18	4.00	4.19	1.95	2.00	1.98	3.90	3.98
			(1.99)	(2.00)	(1.92)	(3.98)	(3.92)	(1.96)	(1.89)	(2.15)	(3.92)	(4.04)
		5.52	1.95	1.98	1.99	3.90	3.97	1.96	2.02	2.01	3.92	4.03
			(1.96)	(1.97)	(1.99)	(3.92)	(3.96)	(1.95)	(1.92)	(2.08)	(3.90)	(4.00)
	bulk SFMO	5.57	2.00	2.00	2.01 ^{a)}	3.99	3.99	1.95	1.95	1.95	3.89	3.89
		2.00 ^{b)}	2.00 ^{b)}	2.00 ^{b)}	4.00 ^{a)}	4.02 ^{a)}	1.94 ^{a)}	1.95 ^{a)}	1.95 ^{a)}	3.88 ^{a)}	3.90 ^{a)}	
		1.98 ^{b)}	2.00 ^{b)}	2.00 ^{b)}	3.96 ^{b)}	4.00 ^{b)}	1.96 ^{b)}	1.94 ^{b)}	1.94 ^{b)}	3.92 ^{b)}	3.88 ^{b)}	
Re	model I	5.57	2.00	2.11	4.00	4.22	1.94	2.02	3.88	4.04		
		5.52	1.97	2.14	3.94	4.28	1.93	2.03	3.86	4.06		
	model II	5.57	2.00	1.99	2.23	4.00	4.22	1.95	2.02	1.97	3.90	3.99
		5.52	1.98	2.00	2.27	3.96	4.27	1.94	2.03	1.97	3.88	4.00
	model III	5.57	2.00	2.04	2.17	4.00	4.21	1.94	2.01	1.99	3.88	4.00
			(1.99)	(2.00)	(1.92)	(3.98)	(3.92)	(1.96)	(1.89)	(2.14)	(3.92)	(4.03)
		5.52	1.98	2.05	2.19	3.96	4.24	1.93	2.01	1.99	3.86	4.00
			(1.97)	(2.02)	(1.92)	(3.94)	(3.94)	(1.94)	(1.90)	(2.15)	(3.88)	(4.05)
	bulk SFRO	5.57	2.00	2.00	4.01	4.01	1.94	1.94	3.88			
		2.01 ^{c)}	2.01 ^{c)}	4.02 ^{c)}	4.02 ^{c)}	1.94 ^{c)}	1.94 ^{c)}	3.88 ^{c)}				

a) Ref. 22; experimental results for bulk SFMO.

b) Ref. 24; experimental results for bulk SFMO.

c) Ref. 37; theoretical results for bulk SFRO.

In Figs. 3 and 4, the DOSs of the SFMO and SFRO UTFs with $a=5.57$ Å are shown, respectively, together with those of the bulk SFMO and SFRO. The DOSs for models with $a=5.52$ Å are almost the same and not shown. Figs. 3(a) and 4(a) are for model I, Figs. 3(b) and 4(b) for model II, Figs. 3(c) and 4(c) for model III, and Figs. 3(d) and 4(d) for the bulk SFXO. The partial DOSs shown in the figures are for the Fe $3d$, Mo $4d$, Re $5d$, O $2p$, and Ti $3d$ orbitals. In the figures, the zero of the energy is taken as the Fermi level, which is shown by the dotted lines. To focus on the partial DOSs of the Fe $3d$, Mo $4d$, and Re $5d$ orbitals, the unit for the DOS is chosen to be states/eV/Fe atom. Note that this choice makes the integrated intensity of the total DOS and partial DOS of O $2p$ orbitals different from figure to figure; in particular, the total DOS and partial DOS of the O $2p$ orbitals in Figs. 3(c) and 4(c) are emphasized.

The calculated DOSs show that all the models are half-metallic. That is, the DOSs of down-spin electrons at the Fermi level are not zero while those of the up-spin electrons are zero. Note that the SFXO UTFs are half-metallic despite the models considered here being extremely thin. This is not trivial; for example, the UTFs of Heusler alloys are not half-metallic.^{56,57)}

Next, we examine the details of the partial DOS. The O $2p$ states extend from -9 to -2 eV. The up-spin Fe $3d$ states of t_{2g} or e_g character also extend over the same energy range and are considerably hybridized with the O $2p$ states. Note that the up-spin Fe $3d$ states are completely occupied. The up-spin Mo $4d$ or Re $5d$ states of t_{2g} character are empty and located at 0.5 eV above the Fermi level. On the other hand, the down-spin Fe $3d$ states of t_{2g} character are partially occupied and hybridized with the Mo $4d$ or Re $5d$ states of t_{2g} character.

It is worth showing the DOS calculated without the on-site Coulomb repulsion U_{eff} to see its effects. The results of calculations for $a=5.57$ Å in which all the on-site Coulomb repulsions are set to zero are shown in Figs. 5 and 6 for $X=\text{Mo}$ and Re , respectively. It is clearly seen that the energy gaps in the DOS for the up-spin electrons are considerably reduced. Nevertheless, the SFXO UTFs are perfectly or almost perfectly half-metallic; model III of the SFMO UTF is not a perfect half metal but is an almost perfect half metal due to a very small but nonvanishing DOS at the Fermi level originating from the up-spin Ti $3d$ states.

In Table II, we show the calculated spin polarizations P defined by $[D_{\uparrow}(E_F) - D_{\downarrow}(E_F)]/[D_{\uparrow}(E_F) + D_{\downarrow}(E_F)]$, where $D_{\sigma}(E_F)$ denotes the DOS of the σ -spin electrons at the Fermi level. The calculated M_{spin} values of the Fe and X atoms are also shown in the table together with the total M_{spin} per Fe atom. For comparison, those calculated without the on-site Coulomb repulsion U_{eff} are shown in parentheses. When the on-site Coulomb repulsion is

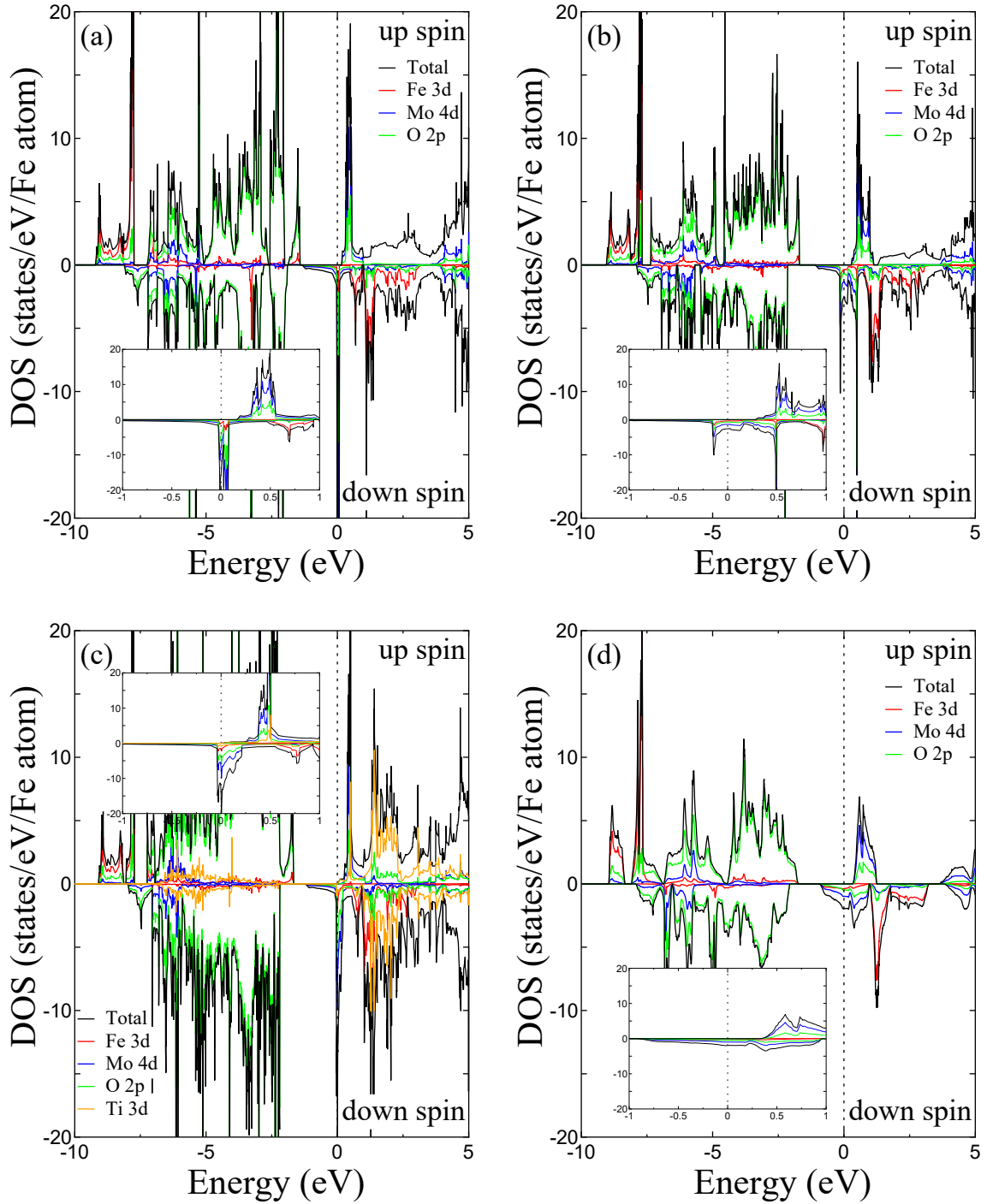


Fig. 3. (Color online) Total and partial DOSs of the SFMO ultrathin films, together with those of their bulk, for the in-plane lattice constant $a=5.57$ Å. Panels (a), (b), and (c) are for models (a) I, (b) II, and (c) III, respectively, and panel (d) is for the bulk. To focus on the partial DOSs of the Fe 3d and Mo 4d orbitals, the unit for the DOS is chosen to be states/eV/Fe atom. The zero of the energy, shown by the dotted line, is taken as the Fermi level. The inset in each panel shows an enlargement around the Fermi level.

taken into account, the spin polarizations are almost 100% for all the models studied here, in

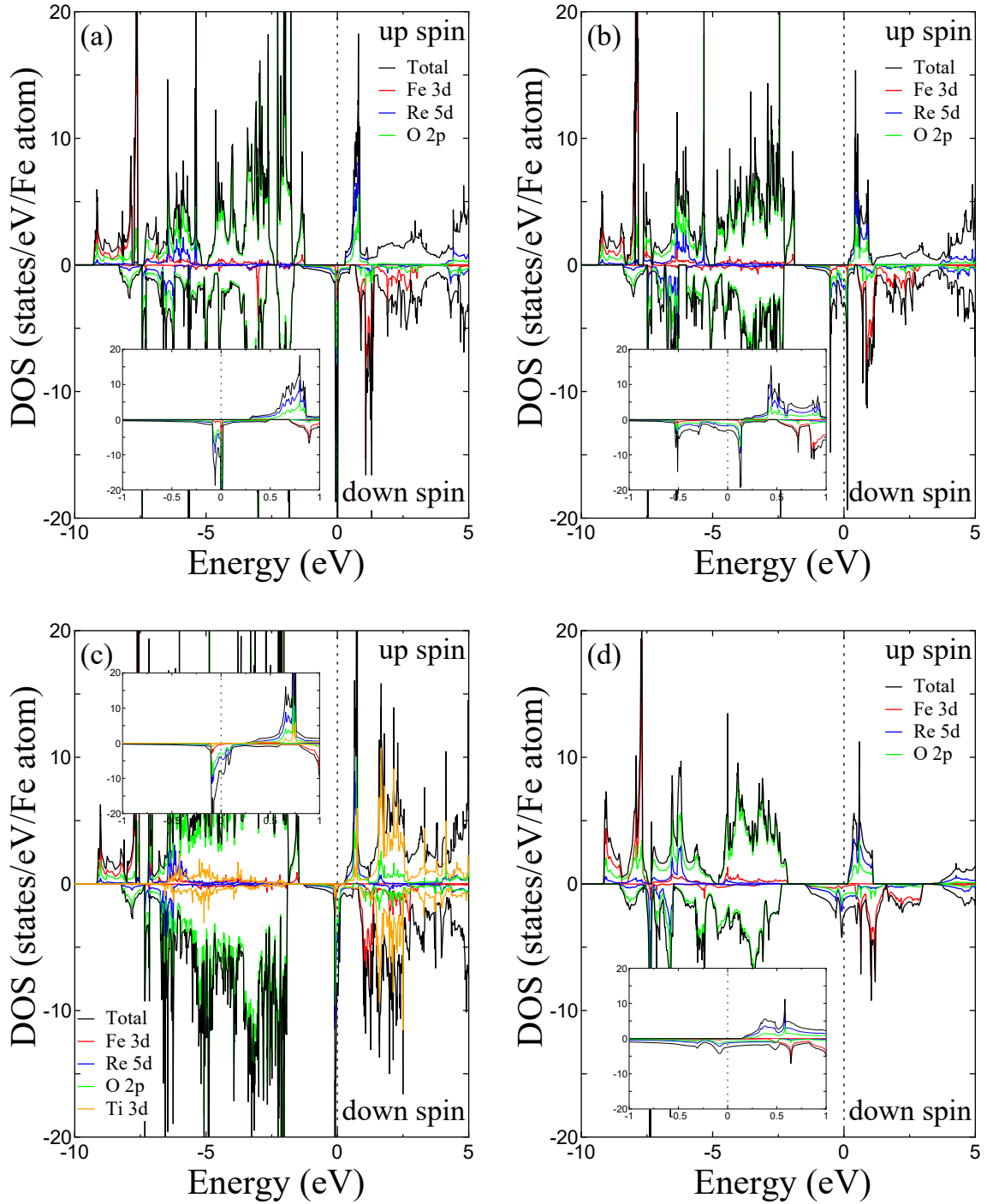


Fig. 4. (Color online) Total and partial DOSs of the SFRO ultrathin films, together with those of their bulk, for the in-plane lattice constant $a=5.57 \text{ \AA}$. Panels (a), (b), and (c) are for models (a) I, (b) II, and (c) III, respectively, and panel (d) is for the bulk. To focus on the partial DOSs of the Fe 3d and Re 5d orbitals, the unit for the DOS is chosen to be states/eV/Fe atom. The zero of the energy, shown by the dotted line, is taken as the Fermi level. The inset in each panel shows an enlargement around the Fermi level.

agreement with the result mentioned above that they are all half-metallic as shown in Figs. 3

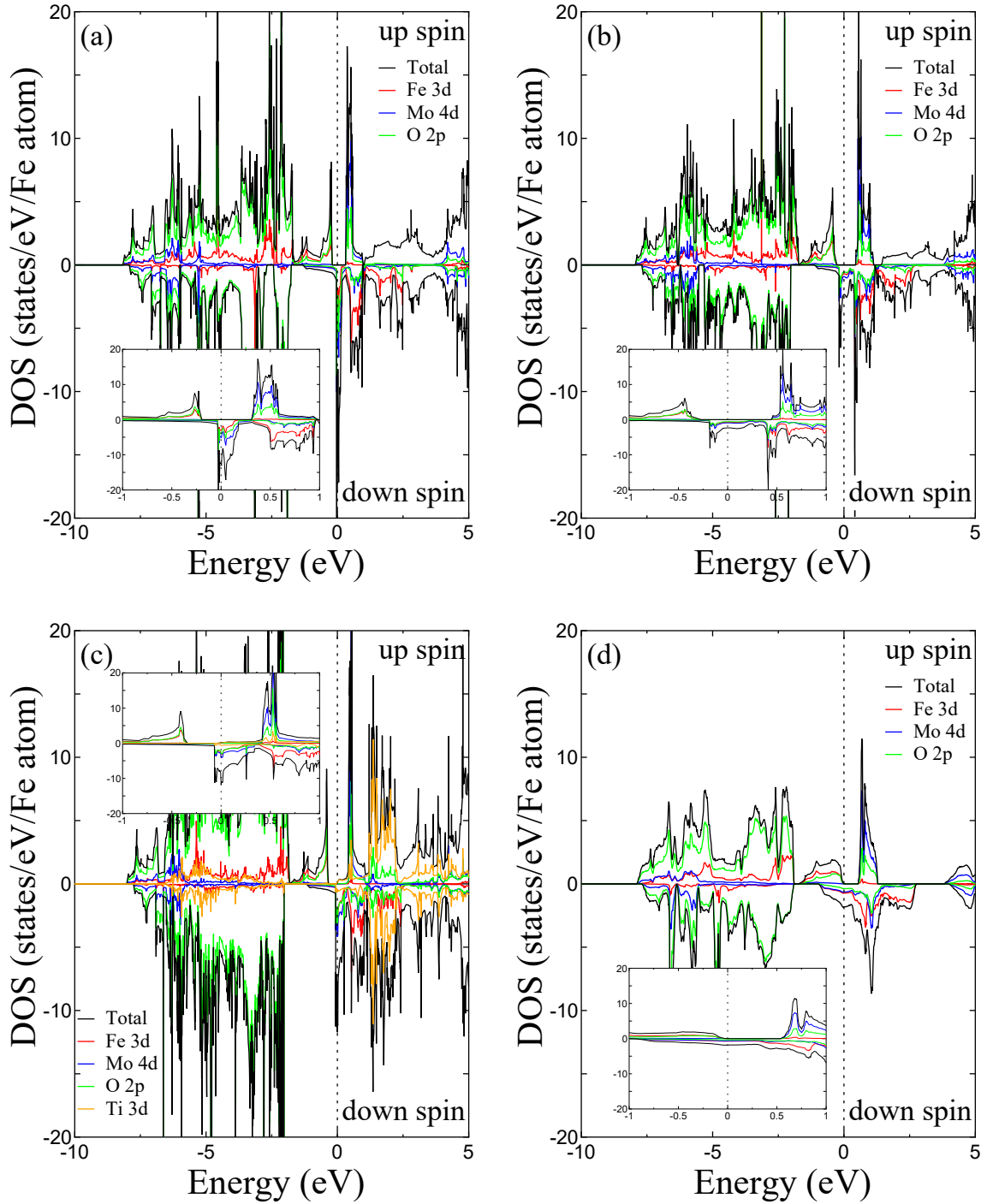


Fig. 5. (Color online) Same as Fig. 3, but all the on-site Coulomb repulsions U_{eff} are set to zero.

and 4. The M_{spin} values of the Fe and X atoms are almost the same for all the models: about $4.2 \mu_B$ for the Fe atoms, about $-0.6 \mu_B$ for the Mo atoms, and about $-1.3 \mu_B$ for the Re atoms. The total M_{spin} per Fe atom is $4.0 \mu_B$ for $X=\text{Mo}$ and $3.0 \mu_B$ for $X=\text{Re}$; note that all the total M_{spin} values are integers, reflecting the fact that they are all half-metallic. On the other

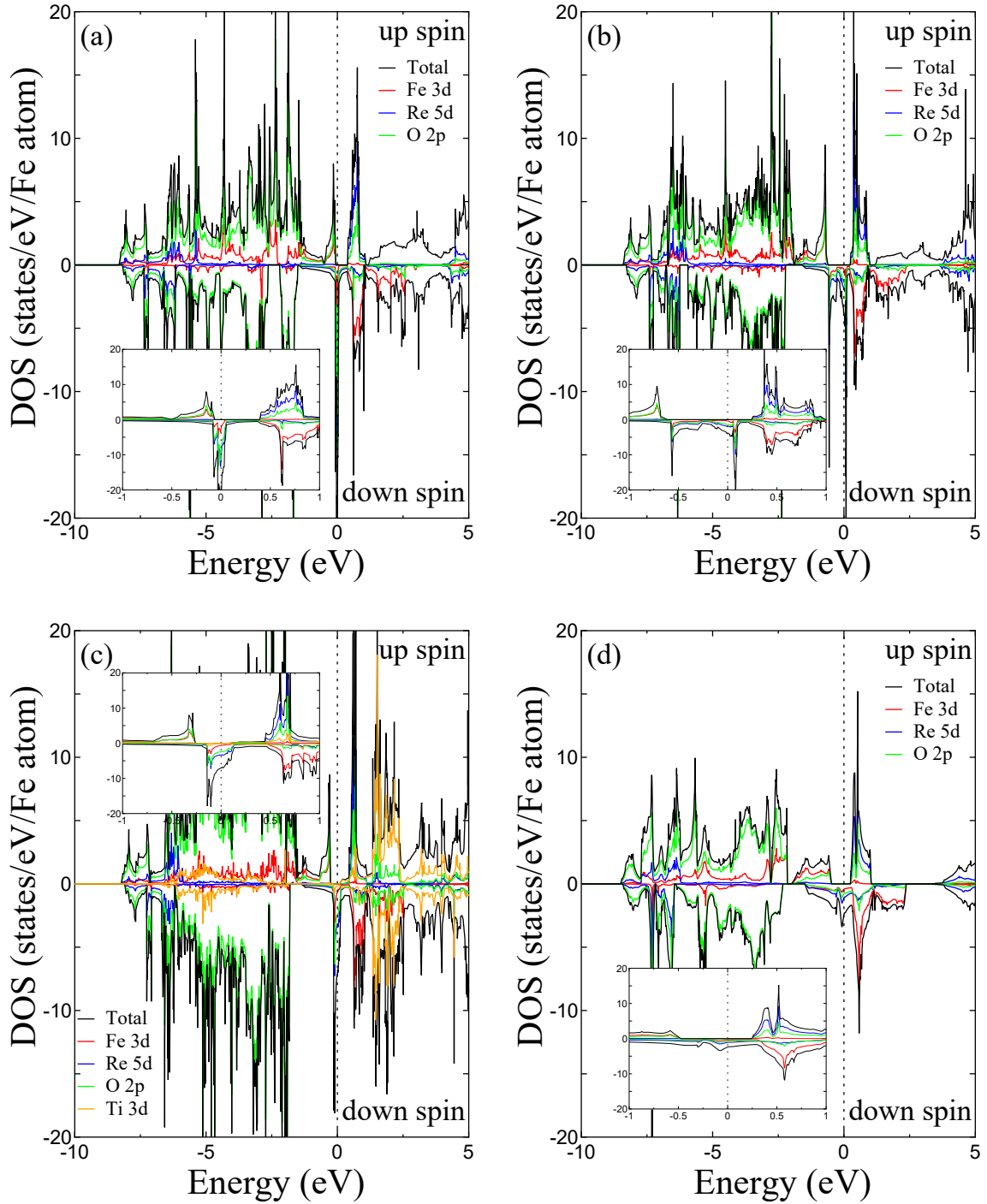


Fig. 6. (Color online) Same as Fig. 4, but all the on-site Coulomb repulsions U_{eff} are set to zero.

hand, when the on-site Coulomb repulsion is neglected, the half-metallicity of model III of the SFMO UTF with $a=5.52 \text{ \AA}$ is lost; the spin polarization of the system is 0.56, although the other systems remain perfectly or almost perfectly half-metallic.

To study the robustness of the half-metallicity of the SFXO UTFs, we optimized the

structure of model I by changing the in-plane lattice constant a from 5.0 to 5.9 Å. As a result, when the on-site Coulomb repulsion is taken into account, we found that model I remains half-metallic between $a=5.05$ and 5.65 Å for $X=\text{Mo}$ and between $a=5.10$ and 5.80 Å for $X=\text{Re}$. That is, the SFXO UTFs remain half-metallic in a lattice constant range of over 0.5 Å. This indicates that the SFXO UTFs are sufficiently robust against the strain that may be induced by various external conditions. In particular, taking account of the fact that the lattice constant of the bulk SFXO is $a=5.57$ Å, the SFXO UTFs, especially the SFRO UTFs, are considerably robust against the strain. On the other hand, when the on-site Coulomb repulsion is neglected, we found that model I remains half-metallic between $a=5.50$ and 5.85 Å for $X=\text{Mo}$ and between $a=5.47$ and 5.90 Å for $X=\text{Re}$. The range in which the systems remain half-metallic is reduced to 0.3 Å. In particular, since the lower bound of the range for the SFMO UTF, 5.50 Å, is close to the lattice constant of STO, 5.52 Å, whether the system remains half-metallic or not is a subtle problem; this is most likely the reason why the half-metallicity of model III of the SFMO UTF with $a=5.52$ Å is lost, as already mentioned. In contrast, the SFRO UTF is still robust against strain because the lower bound of its range, 5.47 Å, is sufficiently small under usual conditions.

Table II. Spin polarizations P and spin magnetic moments of Fe and X atoms and total spin magnetic moments per Fe atom (in μ_B) for models I, II, and III of the SFXO ultrathin films, together with those for the bulk SFXO. The results of calculations without the on-site Coulomb repulsion U_{eff} are shown in parentheses for comparison.

X	System	a	P	Fe	X	total
Mo	model I	5.57	1.00 (1.00)	4.21 (3.77)	-0.66 (-0.48)	4.00 (4.00)
		5.52	1.00 (1.00)	4.20 (3.76)	-0.65 (-0.46)	4.00 (4.00)
	model II	5.57	1.00 (1.00)	4.20 (3.77)	-0.64 (-0.44)	4.00 (4.00)
		5.52	1.00 (1.00)	4.20 (3.76)	-0.64 (-0.43)	4.00 (4.00)
	model III	5.57	1.00 (0.98)	4.20 (3.79)	-0.58 (-0.40)	4.00 (3.99)
		5.52	0.99 (0.56)	4.26 (2.33)	-0.65 (-0.63)	4.01 (1.61)
	bulk SFMO	5.57	1.00 (1.00)	4.22 (3.78)	-0.61 (-0.37)	4.00 (4.00)
	Re	model I	5.57	1.00 (1.00)	4.21 (3.78)	-1.34 (-1.15)
5.52			1.00 (1.00)	4.19 (3.74)	-1.32 (-1.11)	3.00 (3.00)
model II		5.57	1.00 (1.00)	4.19 (3.75)	-1.31 (-1.11)	3.00 (3.00)
		5.52	1.00 (1.00)	4.18 (3.73)	-1.31 (-1.09)	3.00 (3.00)
model III		5.57	1.00 (1.00)	4.19 (3.77)	-1.26 (-1.05)	3.00 (3.00)
		5.52	1.00 (1.00)	4.18 (3.74)	-1.25 (-1.03)	3.00 (3.00)
bulk SFRO		5.57	1.00 (1.00)	4.17 (3.73)	-1.20 (-0.96)	3.00 (3.00)

Finally, we show the calculated MAEs for models I and III in Table III. The MAEs are all positive, implying perpendicular magnetic anisotropy. The MAEs of the SFMO UTFs are 5.0 and 0.6 meV/Fe atom for $a=5.57$ and 5.52 Å, respectively. The MAE is further reduced by adding the STO insulating layer as a substrate. On the other hand, the MAEs of the SFRO UTFs are very large; the MAEs for model I are 28.2 and 15.0 meV/Fe atom for $a=5.57$ and 5.52 Å, respectively. This is two orders of magnitude larger than the MAE calculated for the bulk SFRO by Chen et al. also shown in Table III, which is 0.1 meV/Fe atom;³⁸⁾ because of the nearly cubic symmetry of the bulk SFRO, its MAE is substantially smaller than that in the UTFs, in which the high symmetry is lost due to the existence of the surface or interface. Also, the MAE of the SFRO UTFs is significantly larger than the giant MAE of 9 meV/Co atom observed in the system of single Co atoms deposited on a Pt(111) underlayer.⁷¹⁾ The MAEs of the SFRO UTFs are reduced when the STO insulating layer is added as a substrate. Nevertheless, its MAEs are still very large.

Table III. MAEs (meV/Fe atom) of models I and III for different in-plane lattice constants a (in Å).

X	System	a	MAE
Mo	model I	5.57	5.0
		5.52	0.6
	model III	5.57	2.4
		5.52	0.3
Re	model I	5.57	28.2
		5.52	15.0
	model III	5.57	9.8
		5.52	5.5
	bulk SFRO	5.57	0.1 ^{a)}

a) Ref. 38; MAE calculated for bulk SFRO.

4. Conclusions

We have studied the SFXO UTFs and their heterostructures with a STO substrate by first-principles calculations based on density functional theory. The UTFs and their heterostructures are all half-metallic despite being extremely thin. The FeO_6 and XO_6 octahedra in the SFXO UTFs are elongated along the perpendicular direction. It is also shown that the half-metallicity of the SFXO UTFs is robust against in-plane strain. The MAEs of the SFXO UTFs

are all positive, implying perpendicular magnetic anisotropy. In particular, the MAEs of the SFRO UTFs are found to be very large.

Acknowledgment

We would like to thank T. Oikawa for helpful discussions and comments.

References

- 1) *Handbook of Spintronics*, ed. Y. Xu, D. D. Awschalom, and J. Nitta (Springer, Dordrecht, 2015).
- 2) S. A. Wolf, D. D. Awschalom, R. A. Buhrman, J. M. Daughton, S. von Molnar, M. L. Roukes, A. Y. Chtchelkanova, and D. M. Treger, *Science* **294**, 1488 (2001).
- 3) M. Julliere, *Phys. Lett. A* **54**, 225 (1975).
- 4) T. Miyazaki and N. Tezuka, *J. Magn. Magn. Mater.* **139**, L2341 (1995).
- 5) J. S. Moodera, L. R. Kinder, T. M. Wong, and R. Meservey, *Phys. Rev. Lett.* **74**, 3273 (1995).
- 6) M. Bowen, V. Cros, F. Petroff, A. Fert, C. Martínez Boubeta, J. L. Costa-Krämer, J. V. Anguita, A. Cebollada, F. Briones, J. M. de Teresa, L. Morellón, M. R. Ibarra, F. Güell, F. Peiró, and A. Cornet, *Appl. Phys. Lett.* **79**, 1655 (2001).
- 7) S. Yuasa, T. Nagahama, A. Fukushima, Y. Suzuki, and K. Ando, *Nat. Mater.* **3**, 868 (2004).
- 8) S. S. P. Parkin, C. Kaiser, A. Panchula, P. M. Rice, B. Hughes, M. Samant, and S.-H. Yang, *Nat. Mater.* **3**, 862 (2004).
- 9) D. D. Djayaprawira, K. Tsunekawa, M. Nagai, H. Maehara, S. Yamagata, N. Watanabe, S. Yuasa, Y. Suzuki, and K. Ando, *Appl. Phys. Lett.* **86**, 092502 (2005).
- 10) S. Yuasa, Y. Suzuki, T. Katayama, and K. Ando, *Appl. Phys. Lett.* **87**, 242503 (2005).
- 11) Y. M. Lee, J. Hayakawa, S. Ikeda, F. Matsukura, and H. Ohno, *Appl. Phys. Lett.* **90**, 212507 (2007).
- 12) W. H. Butler, X.-G. Zhang, T. C. Schulthess, and J. M. MacLaren, *Phys. Rev. B* **63**, 054416 (2001).
- 13) J. Mathon and A. Umerski, *Phys. Rev. B* **63**, 220403(R) (2001).
- 14) S. Yuasa and D. D. Djayaprawira, *J. Phys. D: Appl. Phys.* **40**, R337 (2007).
- 15) I. Galanakis and P. H. Dederichs, in *Half-Metallic Alloys*, ed. I. Galanakis and P. H. Dederichs (Springer, Berlin Heidelberg, 2005) p. 1.
- 16) K. Schwarz, *J. Phys. F: Met. Phys.* **16**, L211 (1986).
- 17) R. J. Soulen Jr., J. M. Byers, M. S. Osofsky, B. Nadgorny, T. Ambrose, S. F. Cheng, P. R. Broussard, C. T. Tanaka, J. Nowak, J. S. Moodera, A. Barry, and J. M. D. Coey, *Science* **282**, 85 (1998).

- 18) Z. Zhang and S. Satpathy, Phys. Rev. B **44**, 13319 (1991).
- 19) Y. S. Dedkov, U. Rüdiger, and G. Güntherodt, Phys. Rev. B **65**, 064417 (2002).
- 20) B.-G. Liu, in *Half-Metallic Alloys*, ed. I. Galanakis and P. H. Dederichs (Springer, Berlin Heidelberg, 2005) p. 267.
- 21) J.-H. Park, E. Vescovo, H.-J. Kim, C. Kwon, R. Ramesh, and T. Venkatesan, Nature **392**, 794 (1998).
- 22) K.-I. Kobayashi, T. Kimura, H. Sawada, K. Terakura, and Y. Tokura, Nature **395**, 677 (1998).
- 23) K.-I. Kobayashi, T. Kimura, Y. Tomioka, H. Sawada, K. Terakura, and Y. Tokura, Phys. Rev. B **59**, 11159 (1999).
- 24) Y. Tomioka, T. Okuda, Y. Okimoto, R. Kumai, K.-I. Kobayashi, and Y. Tokura, Phys. Rev. B **61**, 422 (2000).
- 25) D. D. Sarma, P. Mahadevan, T. Saha-Dasgupta, S. Ray, and A. Kumar, Phys. Rev. Lett. **85**, 2549 (2000).
- 26) Y. Moritomo, Sh. Xu, T. Akimoto, A. Machida, N. Hamada, K. Ohoyama, E. Nishibori, M. Takata, and M. Sakata, Phys. Rev. B **62**, 14224 (2000).
- 27) J. Kanamori and K. Terakura, J. Phys. Soc. Jpn. **70**, 1433 (2001).
- 28) Z. Fang, K. Terakura, and J. Kanamori, Phys. Rev. B **63**, 180407 (2001).
- 29) H. Wu, Phys. Rev. B **64**, 125126 (2001).
- 30) I. V. Solovyev, Phys. Rev. B **65**, 144446 (2002).
- 31) T. Saitoh, M. Nakatake, A. Kakizaki, H. Nakajima, O. Morimoto, Sh. Xu, Y. Moritomo, N. Hamada, and Y. Aiura, Phys. Rev. B **66**, 035112 (2002).
- 32) H.-T. Jeng and G. Y. Guo, Phys. Rev. B **67**, 094438 (2003).
- 33) Z. Szotek, W. M. Temmerman, A. Svane, L. Petit, and H. Winter, Phys. Rev. B **68**, 104411 (2003).
- 34) N. Auth, G. Jakob, W. Westerburg, C. Ritter, I. Bonn, C. Felser, and W. Tremel, J. Magn. Mater. **272**, e607 (2004).
- 35) H. Kato, T. Okuda, Y. Okimoto, Y. Tomioka, K. Oikawa, T. Kamiyama, and Y. Tokura, Phys. Rev. B **69**, 184412 (2004).
- 36) V. Kanchana, G. Vaitheeswaran, M. Alouani, and A. Delin, Phys. Rev. B **75**, 220404 (2007).

- 37) Y. Zhang and V. Ji, *Physica B* **407**, 912 (2012).
- 38) X. Chen, D. Parker, K. P. Ong, M.-H. Du, and D. J. Singh, *Appl. Phys. Lett.* **102**, 102403 (2013).
- 39) R. Lu, H. Wu, Y. Qian, E. Kan, Y. Liu, W. Tan, C. Xiao, and K. Deng, *Solid State Commun.* **191**, 70 (2014).
- 40) T. Manako, M. Izumi, Y. Konishi, K. Kobayashi, M. Kawasaki, and Y. Tokura, *Appl. Phys. Lett.* **74**, 2215 (1999).
- 41) H. Asano, S. B. Ogale, J. Garrison, A. Orozco, Y. H. Li, E. Li, V. Smolyaninova, C. Galley, M. Downes, M. Rajeswari, R. Ramesh, and T. Venkatesan, *Appl. Phys. Lett.* **74**, 3696 (1999).
- 42) H. Q. Yin, J.-S. Zhou, J.-P. Zhou, R. Dass, J. T. McDevitt, and J. B. Goodenough, *Appl. Phys. Lett.* **75**, 2812 (1999).
- 43) W. Westerburg, D. Reisinger, and G. Jakob, *Phys. Rev. B* **62**, 767 (2000).
- 44) H. Asano, M. Osugi, Y. Kohara, D. Higashida, and M. Matsui, *Jpn. J. Appl. Phys.* **40**, 4883 (2001).
- 45) M. Besse, F. Pailloux, A. Barthélémy, K. Bouzehouane, A. Fert, J. Olivier, O. Durand, F. Wyczisk, R. Bisaro, and J.-P. Contour, *J. Cryst. Growth* **241**, 448 (2002).
- 46) R. P. Borges, S. Lhostis, M. A. Bari, J. J. Versluijs, J. G. Lunney, J. M. D. Coey, M. Besse, and J.-P. Contour, *Thin Solid Films* **429**, 5 (2003).
- 47) A. Venimadhav, F. Sher, J. P. Attfield, and M. G. Blamire, *J. Magn. Magn. Mater.* **269**, 101 (2004).
- 48) T. Fix, D. Stoeffler, S. Colis, C. Ulhaq, G. Versini, J. P. Vola, F. Huber, and A. Dinia, *J. Appl. Phys.* **98**, 023712 (2005).
- 49) H. Suwaki, T. Yamaguchi, W. Sakamoto, T. Yogo, K. Kikuta, and S. Hirano, *J. Magn. Magn. Mater.* **295**, 230 (2005).
- 50) R. Boucher, *J. Phys. Chem. Solids* **66**, 1020 (2005).
- 51) H. Jalili, N. F. Heinig, and K. T. Leung, *Phys. Rev. B* **79**, 174427 (2009).
- 52) H. Jalili, N. F. Heinig, and K. T. Leung, *J. Chem. Phys.* **132**, 204701 (2010).
- 53) D. Kumar and D. Kaur, *Physica B* **405**, 3259 (2010).
- 54) N. Kumar, P. Misra, R. K. Kotnala, A. Gaur, and R. S. Katiyar, *J. Phys. D: Appl. Phys.* **47**, 065006 (2014).

- 55) Y. Zhang, V. Ji, and K.-W. Xu, *Surf. Interface Anal.* **48**, 1040 (2016).
- 56) I. Galanakis, *J. Phys.: Condens. Matter* **14**, 6329 (2002).
- 57) G. A. de Wijs and R. A. de Groot, *Phys. Rev. B* **64**, 020402 (2001).
- 58) C. T. Tanaka, J. Nowak, and J. S. Moodera, *J. Appl. Phys.* **86**, 6239 (1999).
- 59) S. Suzuki and K. Nakao, *J. Phys. Soc. Jpn.* **66**, 3881 (1997).
- 60) S. Suzuki and K. Nakao, *J. Phys. Soc. Jpn.* **69**, 532 (2000).
- 61) S. Suzuki and K. Nakao, *J. Phys. Soc. Jpn.* **68**, 1982 (1999).
- 62) D. E. Parry, *Surf. Sci.* **49**, 433 (1975).
- 63) F. E. Harris, *Int. J. Quantum Chem.* **68**, 385 (1998).
- 64) J. P. Perdew, K. Burke, and M. Ernzerhof, *Phys. Rev. Lett.* **77**, 3865 (1996).
- 65) V. I. Anisimov, J. Zaanen, and O. K. Andersen, *Phys. Rev. B* **44**, 943 (1991).
- 66) S. L. Dudarev, G. A. Botton, S. Y. Savrasov, C. J. Humphreys, and A. P. Sutton, *Phys. Rev. B* **57**, 1505 (1998).
- 67) I. I. Piyanzina, T. Kopp, Y. V. Lysogorskiy, D. A. Tayurskii, and V. Eyert, *J. Phys.: Condens. Matter* **29**, 095501 (2017).
- 68) D. M. Ceperley and B. J. Alder, *Phys. Rev. Lett.* **45**, 566 (1980).
- 69) J. P. Perdew and Y. Wang, *Phys. Rev. B* **45**, 13244 (1992).
- 70) L.-K. Hua and Y. Wang, *Applications of Number Theory to Numerical Analysis* (Springer-Verlag, Berlin, 1981).
- 71) P. Gambardella, S. Rusponi, M. Veronese, S. S. Dhesi, C. Grazioli, A. Dallmeyer, I. Cabria, R. Zeller, P. H. Dederichs, K. Kern, C. Carbone, and H. Brune, *Science* **300**, 1130 (2003).